HiSST: International Conference on
High-Speed Vehicle Science Technology

26–29 November 2018, Moscow, Russia

Roughness-induced instabilities leading to transition in a capsule boundary-layer under re-entry conditions

Christian Stemmer [1], Antonio Di Giovanni [2]

Abstract

We investigate roughness-induced transition scenarios for the capsule boundary layer in re-entry type scenarios with Direct Numerical Simulations (DNS). The effect of chemical equilibrium as well as chemical and/or thermal non-equilibrium on the disturbance development in the wake of the distributed roughness patch is investigated. DNS calculations are undertaken to show the non-linear evolution of the roughness wake and its interaction with unsteady disturbances. For the modelling of the high-temperature gas effects with chemical equilibrium as well as with chemical and thermal non-equilibrium, the amplification of the unstable modes does not enter the non-linear stage and transition does not take place. For the present flow parameters of a typical re-entry case, the interactions of the roughness patch with the distributed roughness leads to laminar-turbulent breakdown for the case of chemical non-equilibrium.

Keywords: *hypersonic boundary-layer flow, capsule, roughness, laminar-turbulent transition*

Nomenclature

Latin

D – diameter of the hemispheric forebody (shoulder to shoulder)
f – frequency
h – multiple of fundamental frequency
H – altitude
k – roughness height
k – multiple of fundamental wave number
M – Mach number
p – pressure
R – radius of the hemispheric forebody
Re – Reynolds number
T – temperature
x, y, z – downstream, wall-normal, spanwise coordinate

Greek

δ – boundary-layer thickness
λ – wave length

Subscripts

∞ – free-stream conditions
w – conditions at the wall
z – referring to the spanwise direction

1. Introduction

Roughness-induced laminar-turbulent transition is the only instability mechanism which seems feasible in the absence of classical modal instabilities in re-entry capsule boundary layers. At typical flight angles of attack of 24-30° in the relevant flight regime, the boundary layer is strongly accelerated stabilizing it against TS modes. As the stream lines are only marginally curved, cross-flow instabilities are also not present [1]. Therefore, roughness-induced transition is the most likely scenario on these blunt configurations. Transient-growth analysis for steady (and unsteady) disturbances shows only small amplification rates in the immediate vicinity of an isolated roughness element insufficient for the explanation of transition from laminar to turbulent flow [2].

Investigations in the past have mostly concentrated on isolated (singular) roughness elements (see also Stemmer *et al.* [3, 4] as well as many others, among [5, 6]) and the effect of roughness height on the fact

[1] *Adjunct Teaching Professor, Chair of Aerodynamics and Fluid mechanics, Technical University of Munich, Germany, Christian.Stemmer@aer.mw.tum.de*

[2] *Research Associate, Chair of Aerodynamics and Fluid mechanics, Technical University of Munich, Germany, Antonio.DiGiovanni@aer.mw.tum.de*

whether transition from laminar to turbulent flow is triggered or not. This lead to the formulation of the Re_{kk} criterion [7], where a Reynolds number built with the roughness height and the flow properties at the roughness height location determines the border between laminar flow (Re_{kk} <450) and transition to turbulence (Re_{kk} >450) with an uncertainty of roughly 20%. Recent works have shown that the structure of the roughness might have a severe influence on the roughness wake behaviour. Ablative effects on re-entry capsules lead to roughness heights of about 30-50% δ leading to $Re_{kk} \approx 300 - 600$. The high-temperature gas effects during re-entry at altitudes where transition plays a role in the capsule boundary layer need to be recognized to evaluate the roughness effect (see also Stemmer and Fehn [8] for the flow on the smooth capsule).

The current investigations are directed towards investigating the potential transition phenomena and scenarios invoked by distributed roughnesses which go beyond the recognition of a medium height of the distributed roughness in the Re_{kk} criterion.

The presented work deals with a hemispheric body resembling a generic Apollo-like capsule with a sphere radius of $R = 6m$ and the diameter of $D = 5m$ (from shoulder to shoulder) for a re-entry scenario at Mach number 20. For this flight regime, chemical (and thermal) non-equilibrium effects are palpable and influence the disturbance behaviour during the transitional process. In the present case, distributed roughnesses are modelled locally on the capsule in the outer region where the Reynolds number Re_{kk} is in the range of 200-220, which is subcritical compared with the Reda criterion. First, steady state simulations are presented and in a second stage, three discrete frequencies are introduced at the inflow of a small domain in the vicinity of the roughness patch. The disturbance development is shown for different levels on non-equilibrium modelling.

2. Numerical setup

The three-dimensional, unsteady DNS is conducted with the NSMB code which is described and verified for hypersonic flows in Hoarau *et al.* [9], Stemmer *et al.* [3] and Di Giovanni and Stemmer [10]. The finite-volume code can resolve spatial derivatives with fourth-order accurate finite difference and for the time advancement, a fourth-order accurate, five-stage Runge-Kutta scheme is employed, once the post-shock conditions are established with an AUSM+ and an Euler scheme. The chemical modelling is done using the Park five-species model [11] with (N_2, O_2, NO, N, O) allowing for chemical equilibrium and non-equilibrium conditions [12]. Thermal non-equilibrium is possible through an additional conservation equation for vibrational energy. Details on the chemical and thermal modelling can be found in [13].

The computational grid is rectangular and allows for the accumulation of grid points in the boundary layer. A sponge technique is used for the outflow conditions. The free-stream boundary uses a non-reflective condition and the inflow is prescribed in its conditions as a result of precursor computations of the entire capsule configuration including the bow shock. Laterally, symmetry conditions are applied. The results presented here are obtained using a grid with 1120x160x400 points in downstream (x), wall-normal (y) and spanwise (z) direction. The whole problem consists of ~70 Mio. grid points.

The free-stream conditions in front of the bow shock are detailed in Table 1. This results in conditions which are in the high subsonic to lower supersonic range in the integration domain representing only a small section of the entire capsule flow as described in Di Giovanni and Stemmer [10].

Table 1. Base flow properties

Medium	M	H [km]	p_∞ [Pa]	T_∞ [K]	T_w [K]	Re_∞ [1/m]	D [m]	Re_D
Air	20	57.7	29.9	253.3	1800	$1.98 \cdot 10^6$	6.0	$9.87 \cdot 10^6$

The steady simulation delivers the spatial information on the post-shock conditions. A restricted domain with the roughness patch (as shown in Fig. 1) is used for the boundary-layer simulations which allows for the use of more accurate finite differences in the absence of the bow shock in the integration domain.

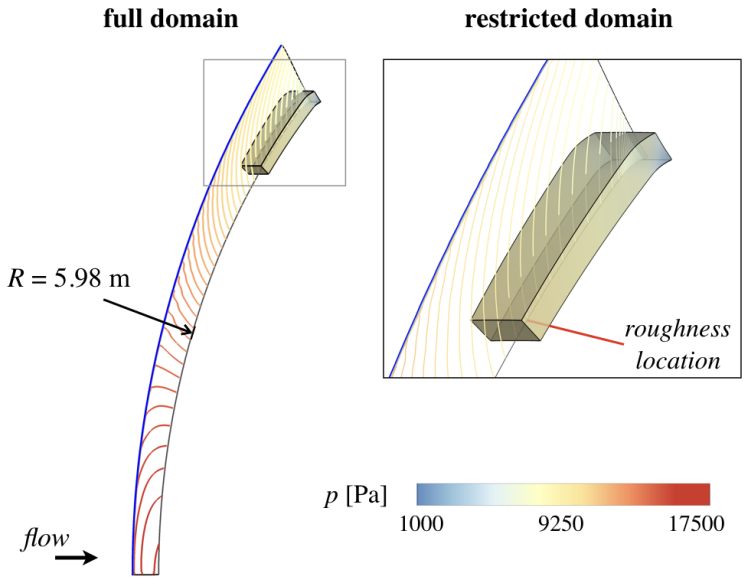

Fig 1. Full domain and partial domain with pressure

A roughness patch (as described in detail in Di Giovanni and Stemmer [10]) is modelled with a discrete number of sine-waves in the downstream stretch of $3.755m \leq x \leq 3.925m$. This results in peaks and valleys skewed relative to the main flow direction (see Fig. 2)

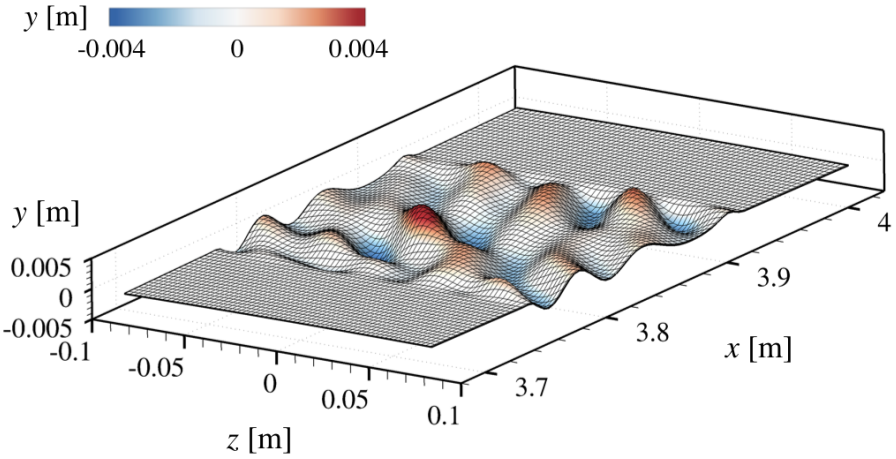

Fig 2. Wall shape for the modelled surface roughness patch (from AIAA 2018-4046)

The disturbances are introduced at the inflow as a sum of 5 spanwise wavenumbers and discrete frequencies for pressure disturbances. Due to the strong acceleration of the flow on the capsule, the flow is modally stable and the introduction of unwanted modes through the pressure-only disturbance in negligible.

3. Results

First, steady results of the topology of the flow over the distributed roughness patch are presented. In a second set of numerical experiments, discrete disturbance frequencies are introduced interacting with the roughness wakes.

To investigate the wake structure for the steady case, spanwise/wall-normal contour plots of the vorticity (Fig. 3) and the temperature (Fig. 4) are shown at $x = 3.935m$. the area of interest includes the largest vortex in the wake at $z = -0.027m$ downstream of the largest peak. The three chemical models employed exhibit the same vortical structure which resembles closely a crossflow vortex as known from three-dimensional subsonic boundary layer flows (see e.g. [14]).

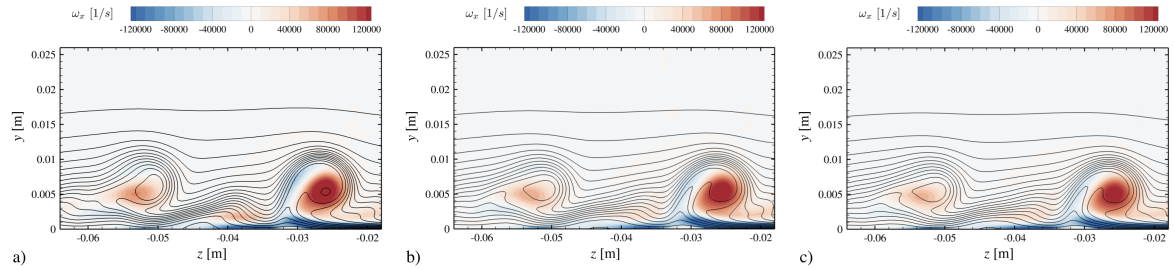

Fig 3. Vorticity (spanwise, wall-normal) at $x = 3.935m$ for (a) chemical equilibrium conditions, (b) chemical non-equilibrium and (c) chemical and thermal non-equilibrium

Contrary to the vorticity, the temperature cross cuts are strongly influenced by the chemical modelling. The equilibrium conditions show the highest temperature values as has to be expected and the cold wall shows full recombination of the atomic nitrogen. The crossflow-like vortex moves hot fluid closer to the wall on the downward-sweep side ($z \leq -0.022m$). The non-equilibrium cases show lower temperatures altogether but stronger temperature gradients at the top and at the lateral sides of the vortex.

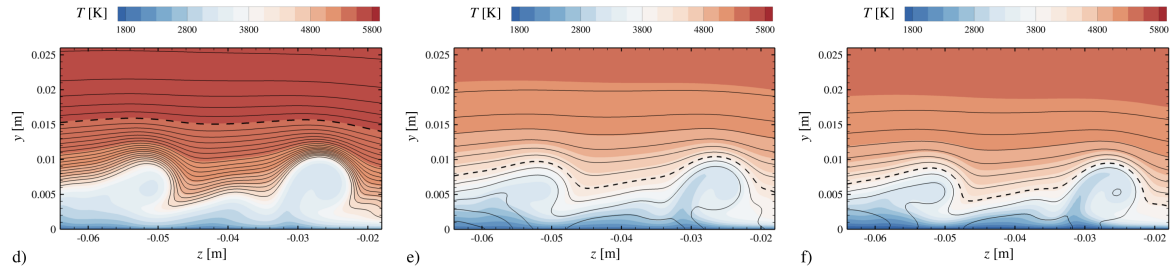

Fig 4. Temperature contours in color (spanwise, wall-normal) at $x = 3.935m$ for (a) chemical equilibrium conditions, (b) chemical non-equilibrium and (c) chemical and thermal non-equilibrium. Isolines are the concentration of atomic nitrogen. dashed line: $c_N = 0.18$, $\Delta c_N = 0.01$

Fig. 5 shows the vortex lines (streamlines through the vortex cores) on the left. It is clearly to be seen, that the strongest vortex stems from the largest roughness. The rotation of the flow is mainly affected by the indentations in front and behind the roughness element. As the flow dips into the indentation at $z = 0.01m$ and $x \approx 3.84m$, the swirling motion of the streamline becomes very strong resulting in the crossflow-type vortex with the largest amplitude in the far field of the roughness patch. The wall heat flux (Fig. 5 (right)) shows the gestation of the streak of high wall heat flux at the downwash side of the vortex at $z \approx 0m$ for $x > 3.95m$.

The evolution of the overall disturbance amplitudes for the three frequencies $f = 11, 33$ and $100\,kHz$ are shown in Fig. 6a) for the chemical non-equilibrium case. The middle frequency of $f = 33\,kHz$ delivers the largest amplitude gain as predicted also by stability investigations (not shown here). The high frequency mode of $f = 100\,kHz$ is linearly damped in the entire domain. The increase in amplitude visible downstream of $x > 4.15m$ is a result of nonlinear amplification due to the presence of the 33 kHz disturbance. For the low frequency of $f = 11\,kHz$, the amplification is not as large as in the case

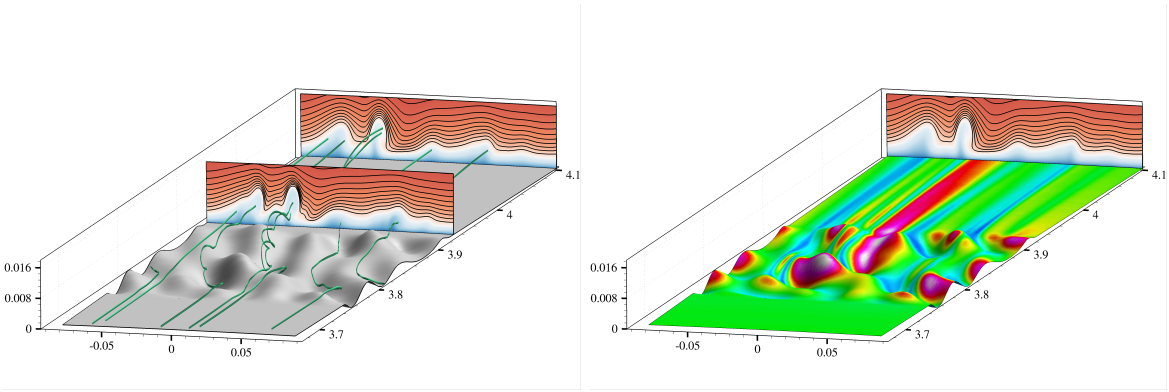

Fig 5. Flow evolution over the roughness for chemical equilibrium flow: (left) vortex cores (green lines) and temperature isocontours at the end of the roughness patch at $x = 3.939m$ and at $x = 4.105m$ and (right) the corresponding heat flux at the wall.

for the middle frequency, but the area of amplification is larger and for $x > 4.6m$, the amplitude for this frequency overtakes the $f = 33\,kHz$ case, which is already on the decline. Results for a wind tunnel experiment at TU Braunschweig with $Ma = 5.9$ and cold conditions are documented in [10, 15].

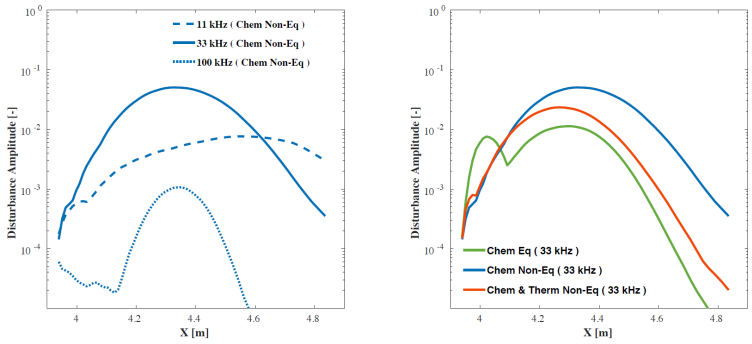

Fig 6. Disturbance amplitude development for (a) chemical non-equilibrium conditions with varying frequencies, and (b) comparison of chemical modelling approaches for a single frequency

For the frequency which shows the largest amplitude gain ($f = 33\,kHz$), the amplitude development of the chemical non-equilibrium case is compared with a chemical equilibrium case and a chemical and thermal non-equilibrium case. As shown in Fig. 6b), the inclusion of chemical non-equilibrium effects boosts the amplification by a factor of 5 compared to the equilibrium case, whereas an additional consideration of the thermal non-equilibrium effects leads to a decrease compared to the chemical non-equilibrium case by a factor of 2-3. The chemical equilibrium disturbance development shows an initial local maximum for $x \approx 4m$, which is not present for the other chemical models. Investigations in [10] have shown, that the disturbances emanating from the roughness patch are dominated by the wake of the highest roughness peak in general. For the mentioned case, the near field in the chemical equilibrium case shows a very short disturbance growth from the wake of the second largest peak up to $x = 4.1m$, which is located at a different spanwise position than the maxima at $x \approx 4.4m$. The disturbance development peaks around $x = 4.4m$ for all chemical models, although at very different amplitudes.

The detailed disturbance development as a result of a spatio-temporal Fourier analysis (Fig. 7) delivers amplitudes (maximum in wall-normal direction) for modes (h,k), where h is the multiple of the fundamental disturbance frequency $f = 11\,kHz$ and k is the multiple of the fundamental spanwise wave

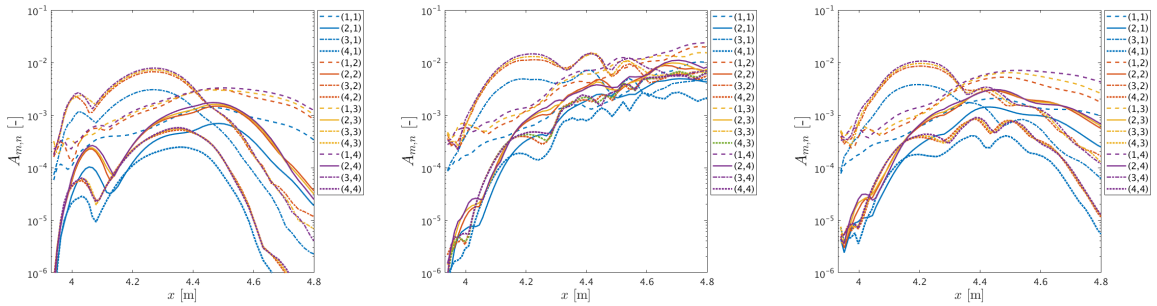

Fig 7. Detailed disturbance amplitude development for (a) chemical equilibrium conditions, (b) chemical non-equilibrium and (c) chemical and thermal non-equilibrium

number $(2\pi)/\lambda_z$ (signifying the spanwise extent of the roughness patch). Shown are frequencies of $11(1), 22(2), 33(3)$ and $44(4)$ kHz with the values of h in the bracket. The disturbed frequencies are 1 and 3 where, again, the different amplifications already present in Fig. 6 are noticeable. It is evident, that the chemical non-equilibrium case (subfigure (b)) delivers the highest disturbance amplitudes for the far range of $x \leq 4.5m$. All spanwise wave numbers are equally involved in the disturbance growth.

As the largest amplitudes of the three-dimensional modes $3, k$ $(2 < k < 4)$ reach non-linear amplitudes around $x \approx 4.25$ for the chemical non-equilibrium case, the laminar flow starts breaking down to turbulence. First, for $4.25 < x < 4.35$, the amplitudes for $f = 33\,kHz$ $(h = 3)$ decrease somewhat, before they undergo a second regime of amplification $(x > 4.32)$ where all other frequencies and wave numbers are involved leading to breakdown. For the chemical equilibrium and the chemical and thermal non-equilibrium case, the amplitudes remain linear and decrease for $x > 4.25$ without further being amplifies. No breakdown could be observed for theses cases, although the inflow disturbance amplitudes where identical in all cases.

For the chemical non-equilibrium case, the flow in the wake of the roughness patch is analysed for vortical structures with the help of the Q-criterion. The main crossflow-type vortex $(z \approx -0.02m)$ develops vortex rings $(4.1m \leq x \leq 4.3m)$ which resembles the non-linear development shown in [14]. In three-dimensional boundary layers, crossflow vortives are subject to a lateral velocity in the boundary layer. In this case, there is just the wrapping of the vortex without a three-dimensional lateral velocity in the entire boundary layer. This might be the explanation, why in three-dimensional crossflow breakdown scenarios, the vortex exhibits the nonlinear development of 'fingers' just on one side. Here, the 'fingers' come from both sides joining at the top, closing the circle to an omega-shape diversification of the vortex. Downstream of $x = 4.4m$ the amplitudes become non-linear and the vortex structures break into bits and pieces as familiar from laminar-turbulent transition scenarios. The broken vortex structures approach the shoulder of the capsule at $x = 4.74m$ (blue surface), where the flow is extremely accelerated tearing apart all structures remaining at that point.

4. Conclusions

The influence of chemical and thermal non-equilibrium on the disturbance development in transitional flows on a rough capsule surface at re-entry conditions is shown. The amplitude developments show the necessity to incorporate the complex non-equilibrium modelling aspect into DNS to get the appropriate information on the non-linear disturbance development leading to laminar-turbulent transition on these highly accelerated boundary layers.

The roughness patch with its skewed elements generated through the pseudo-random superposition of discrete sine waves generates a longitudinal vortex which resembles a cross flow vortex as known from three-dimensional subsonic boundary layers. the breakdown of this cross-flow type vortex in the chemical non-equilibrium case is presented and exhibits features similar to the cross-flow vortex breakdown.

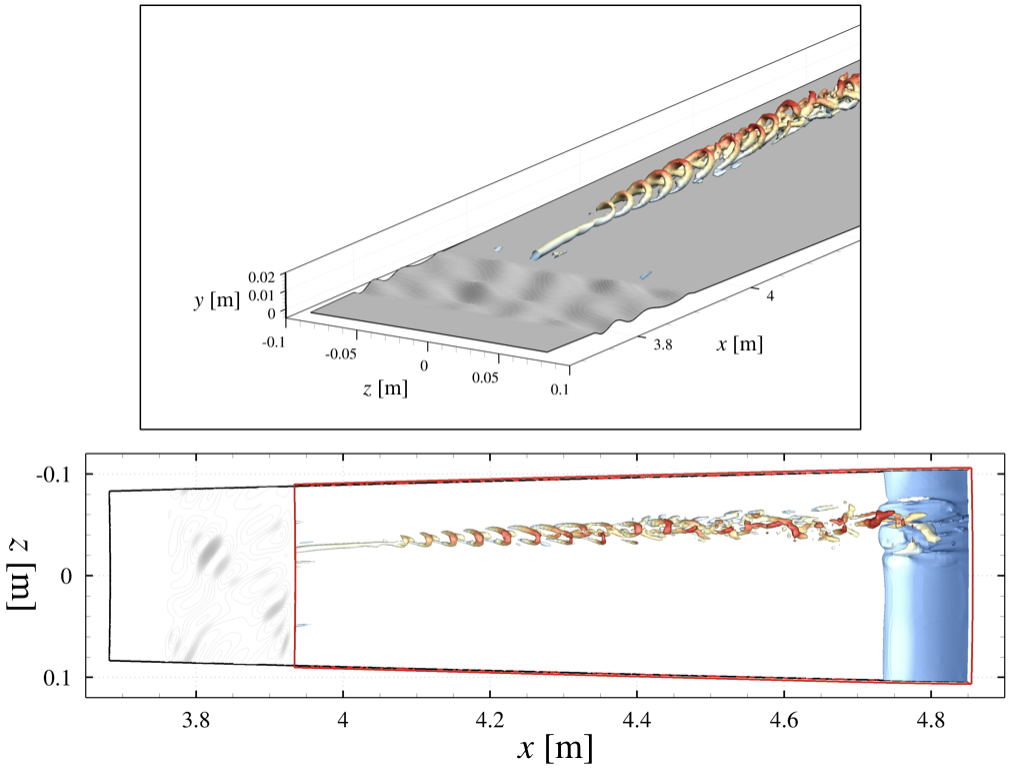

Fig 8. visualization of vortical structures for the chemical non-equilibrium case

Acknowledgements

The work leading to the presented results was conducted under the grant STE 1454/8-2 supported by the German Research Foundation (DFG). The support is greatly acknowledged. The authors gratefully acknowledge the Gauss Centre for Supercomputing e.V. (www.gauss-centre.eu) for providing computing time on the GCS Supercomputer SuperMUC at Leibniz Supercomputing Centre (www.lrz.de).

References

1. A. Theiss, M. Lichtmess, and S. Hein. Local stability analysis of laminar-turbulent boundary layer transition on blunt generic re-entry capsules. In A. Dillmann, G. Heller, E. Krämer, C. Wagner, S. Bansmer, R. Radespiel, and R. Semaan, editors, *New Results in Numerical and Experimental Fluid Mechanics XI*, number 136 in Notes on Numerical Fluid Mechanics and Multidisciplinary Design, pages pp. 279–288. Springer Verlag, Berlin, 2017.

2. A. Theiss, S. Hein, S.R.C. Ali, and R. Radespiel. Wake flow instability studies behind discrete roughness elements on a generic re-entry capsule. *AIAA paper 2016-4382*, 2016.

3. C. Stemmer, M. Birrer, and N.A. Adams. Hypersonic boundary-layer flow with an obstacle in thermochemical equilibrium and nonequilibrium. *Journal of Spacecraft and Rockets*, 54(4):899–915, 2017.

4. C. Stemmer, M. Birrer, and N.A. Adams. Disturbance development in an obstacle wake in a reacting hypersonic boundary layer. *Journal of Spacecraft and Rockets*, 54(4):945–960, 2017.

5. C.-L. Chang, M. Choudhari, B. S. Venkatachari, and F. Li. Effects of cavities and protuberances on transition over hypersonic vehicles. *AIAA Paper 2011-3245*, 2011.

6. M.E. Goldstein, A. Sescu, P.W. Duck, and M. Choudhari. Nonlinear wakes behind a row of elongated roughness elements. *J. Fluid Mech.*, 796:516–557, 2016.

7. D.C. Reda. Review and synthesis of roughness-dominated transition correlations for reentry applications. *Journal of Spacecraft and Rockets*, 39(2):161–167, 2002.
8. C. Stemmer and J. Fehn. High-temperature gas effects at a capsule under re-entry and wind-tunnel conditions. AIAA Fluid Dynamics Conference, Atlanta, *AIAA-paper 2014-2645*, June 2014.
9. Y. Hoarau, D. Pena, J.B. Vos, D. Charbonier, A. Gehri, M. Braza, T. Deloze, and E. Laurendeau. Recent developments of the Navier Stokes Multi Block (NSMB) CFD solver. *AIAA paper 2016-2056*, 2016.
10. A. Di Giovanni and C. Stemmer. Crossflow-type breakdown induced by distributed roughness in the boundary layer of a hypersonic capsule configuration. *Journal of Fluid Mechanics*, 856:470–503, 2018.
11. C. Park. A review of reaction rates in high temperature air. *AIAA Paper 89-1740*, 1989.
12. C. Park. *Nonequilibrium Hypersonic Aerothermodynamics*. John Wiley & Sons, New York, 1990. out of print.
13. C. Stemmer. *Untersuchungen zur Instabilität hypersonischer Grenzschichten unter Berücksichtigung von Hochtemperatureffekten*. Habilitation, Technische Universität München, 2012.
14. P. Wassermann and M. Kloker. Transition mechanisms induced by travelling crossflow vortices in a three-dimensional boundary layer. *Journal of Fluid Mechanics*, 483:67–89, 2003.
15. S.J. Hein, A. Theiss, A. Di Giovanni, C. Stemmer, T. Schilden, W. Schroeder, P. Paredes, M. Choudhari, F. Li, and E. Reshotko. Numerical investigation of roughness effects on transition on spherical capsules, 2018. accepted for publication in the Journal for Spacecraft and Rockets.